A COMPARATIVE STUDY OF HYPERELASTIC CONSTITUTIVE MODELS FOR AN AUTOMOTIVE COMPONENT MATERIAL

Rafael Tobajas[(a)], Daniel Elduque[(b)], Carlos Javierre[(c)], Elena Ibarz[(d)], Luis Gracia[(e)]

[(a),(b),(c),(d),(e)] Department of Mechanical Engineering, University of Zaragoza, C/ María de Luna, 3, 50018 Zaragoza, Spain

[(a)]rafaeltobajasalonso@gmail.com, [(b)]daniel.elduque@gmail.com, [(c)]carlos.javierre@unizar.es, [(d)]eibarz@unizar.es
[(e)]lugravi@unizar.es

ABSTRACT

The use of thermoplastic elastomers has strongly increased in recent decades in order to reduce the size of components in the automotive and aeronautical industries. To design this kind of components, engineers face the challenge of reproducing the behavior of these materials by numerical simulations. This task is not always simple because these materials often have a strongly nonlinear behavior. In this paper an elastomer thermoplastic material has been analyzed and an automotive component has been studied by five numerical simulations with five material constitutive models. This study shows that a careful choice of the constitutive model should be made to obtain reliable results. Although several constitutive models fit well with the experimental data of uniaxial testing, when these are used in actual components, there are significant differences in the obtained results.

Keywords: hiperelasticity, thermoplastic elastomer, finite element method, simulation.

1. INTRODUCTION

Automotive and aeronautical industries consider a future challenge to further increase engine efficiency by decreasing fuel consumption and motor weight. In order to reach it, designers must be able to reduce the size of the engine block and all its components using alternative materials to metals, such as thermoplastic elastomeric polymers. (Drobny, J. G., 2014).

The use of these materials has strongly increased in recent decades due to their good mechanical properties (Štrumberger et al., 2012) (P. Consulting, 2014). In addition to its ease to manufacture complex-shaped components, these materials have great advantages as their high deformation capability, their ability to absorb vibrations and their low cost-weight ratio. (Malloy, 1994).

Despite all their advantages, developing an efficient and durable design with these materials is not an easy task as reproducing their mechanical behavior by simple computational algorithms is not always possible. The constitutive relations between stresses and strains for these materials are nonlinear and time-dependent, and additionally they also experience other effects such as hysteresis and softening (Charlton et al., 1994).

Although hyperelastic constitutive models are the best models to reproduce the nonlinear behavior of these materials, several more complex constitutive models exist in the literature to also take into account other effects. Therefore, the selection of a proper constitutive model remains an engineering challenge to be solved since the behavior of the material has a good fit with any hyperelastic model, the mechanical behavior of the component is often not adapted to the actual behavior.

From these constitutive models, simulations techniques must be used to obtain the stress and strain fields to evaluate the component from an engineering point of view. Simulation is one of the most important fields into the world of engineering due to it is used for such varied sectors such as structural designs and manufacturing studies of plastic parts (Javierre, et al. 2013) (Javierre, et al. 2006) or numerous studies into the food sector (Jiménez, et al. 2014) (Latorre-Biel, et al. 2013).

Finite Element Method (FEM) is a numerical technique currently used in simulation processes for several fields. Specifically, into the mechanical engineering field, it is used for studies of developing of food packaging (Fernandez, et al. 2013), designing of led weatherproof luminaire (Javierre, et al. 2014) or modeling automotive products (Jiménez, et al. 2009) (Ruiz Argáiz, et al. 2008).

In this paper five simulations of a real component used in the automotive industry, based on five different constitutive models of material, have been performed, comparing the corresponding results. In this study, FEM simulations were carried out using the software Abaqus (Version 6.11).

2. MATERIAL DESCRIPTION

An automotive air duct is going to be analyzed in this paper. This component is made of a material called Santoprene 101-73 provided by ExxonMobil (ExxonMobil).

The nonlinear behavior of the material has been described by uniaxial tensile tests like simple tension, planar extension and simple compression. In addition, cyclic behavior information is also provided at different levels of deformation.

To characterize the material, the datasheet and Young modulus value supplied by the manufacturer have been used. This study focuses on the relationship between stress and strain for the first pull deformation, when it is the first time in deforming the material. The Young modulus recommended by the manufacturer in this deformation is E= 29.7 MPa (ExxonMobil). This relationship can also be obtained from the cyclical behavior information of the material, and it is represented by a red line in Figures 1and 2. According to standards (ASTM D412-15a) (ISO 37:2011), the provided values of strain and stress are nominal values.

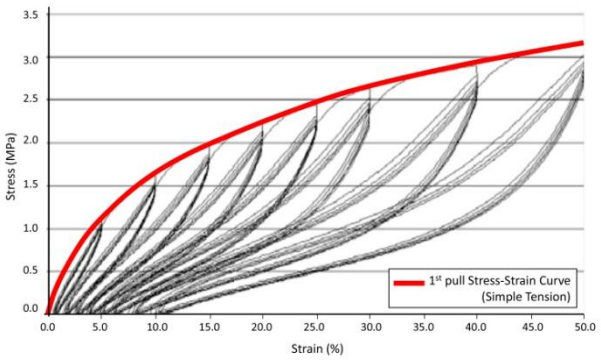

Figure 1: Strain-stress plot of Santoprene 101-73 from manufacturer datasheet (ExxonMobil) for Simple Tension.

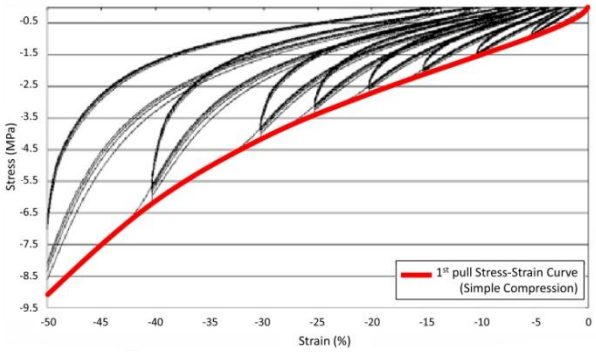

Figure 2: Strain-stress plot of Santoprene 101-73 from manufacturer datasheet (ExxonMobil) for Simple Compression.

In order to obtain values of strain energy density, strain and stress values from the first pull deformation shown in Tables 1 and 2 are used. Strain energy density values were obtained by Equation (1).

$$W = \sum_{i,j=1}^{3} \int_{0}^{\varepsilon_{ij}} \sigma_{ij} d\varepsilon_{ij} \quad (1)$$

Strain, stress and strain energy density (SED) values from the first pull deformation are shown in Tables 1 and 2.

Table 1: Strain-stress values for Santoprene 101-73

First Pull-Simple Tension		
Nominal Strain (%)	Nominal Stress (MPa)	SED (MPa)
0.000	0.000	0.000
0.900	0.345	0.001
2.000	0.615	0.006
3.200	0.859	0.014
4.700	1.084	0.027
6.900	1.338	0.054
8.700	1.516	0.080
9.900	1.623	0.098
12.20	1.792	0.137
13.80	1.913	0.165
14.90	1.981	0.188
17.60	2.122	0.241
18.90	2.193	0.269
19.90	2.232	0.290
23.00	2.374	0.359
24.20	2.422	0.388
25.00	2.451	0.406
28.40	2.585	0.493
29.90	2.631	0.530
33.90	2.768	0.638

Table 2: Strain-stress values for Santoprene 101-73

First Pull-Simple Compression		
Nominal Strain (%)	Nominal Stress (MPa)	SED (MPa)
0.00	0.000	0.0000
-0.90	-0.219	0.0010
-2.00	-0.437	0.0045
-3.20	-0.662	0.0114
-4.70	-0.884	0.0224
-6.90	-1.181	0.0454
-8.70	-1.399	0.0691
-9.90	-1.533	0.0866
-12.20	-1.783	0.1246
-13.80	-1.957	0.1543
-14.90	-2.086	0.1780
-17.60	-2.393	0.2380
-18.90	-2.550	0.2704
-19.90	-2.668	0.2955
-23.00	-3.066	0.3839
-24.20	-3.233	0.4224
-25.00	-3.338	0.4471
-28.40	-3.854	0.5715
-29.90	-4.088	0.6291

3. COMPONENT AND SIMULATIONS DESCRIPTION

The component is an air duct for a combustion engine that has a length of 100 mm and the diameter of the inlet and outlet is 24 mm. In the central area it is formed by five bellows where the maximum diameter is 29 mm and the minimum diameter is 24 mm. The wall thickness is 2 mm. Its geometry is shown in Figure 3.

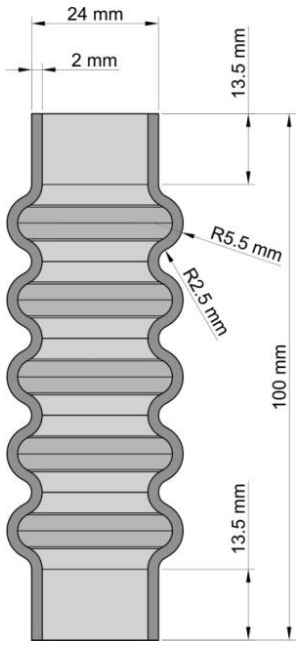

Figure 3: Geometry of the component

The simulation consists of subjecting the component to a prescribed compression deformation of 15 mm in its own axis direction (Figure 4).

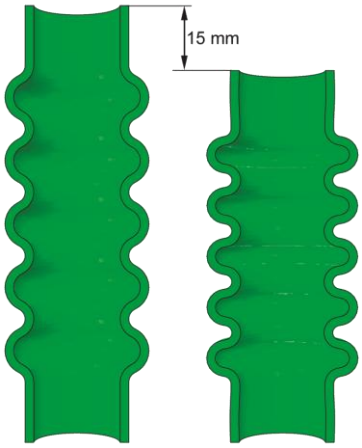

Figure 4: Prescribed deformation in the component

The finite element model was made from a 2D section of the component wall. The 2D section was meshed with 4-node quadrilateral axisymmetric element (CAX4H, Abaqus) (Abaqus Analysis User's Manual, 2011). A radial sweeping from the axis of the duct was used to generate the 3D model (Figure 5). A sensitivity analysis, checking the strain energy convergence, was performed in order to obtain the appropriate mesh size. The mesh consists of 1148 elements and 4027 nodes.

Several simulations with different constitutive models of material are done to study the mechanical behavior of the component.

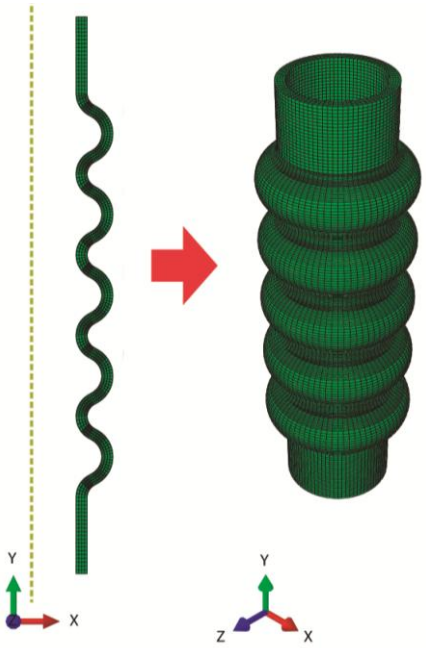

Figure 5: Finite element model of the component

Firstly, a simulation with Elastic material model with E=29.7 MPa was carried out (see Figure 6) to obtain the maximum and minimum strain values in the component. These values are shown in Table 3.

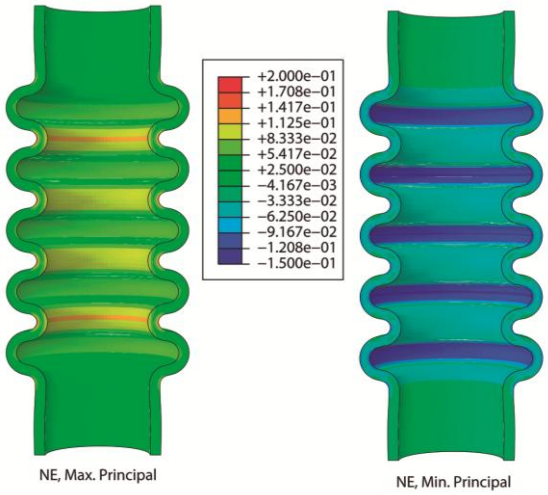

Figure 6: Simulation with Elastic material model (E=29.7 MPa). Strain results

Table 3: Max. and min. strains for the simulation with Elastic material model (E=29.7 MPa).

Max ppal strain (%)	Min. ppal. Strain (%)
19.34	-13.94

Then, the constants of hyperelastic models are going to be fitted for each model and then the simulations with these models are going to be carried out to compare the results.

4. HYPERELASTICITY

The hyperelastic constitutive models are mathematical models that attempt to simulate the behavior of materials whose stress strain relationship is nonlinear.

Usually these models are represented by strain energy density function W which is formulated as a function depending on different magnitudes associated to the strain field and the material constants, in the way:

$$W = W(\boldsymbol{F}) = W(\lambda_1, \lambda_2, \lambda_3) = W(I_1, I_2, I_3) \quad (2)$$

where $\lambda_1, \lambda_2, \lambda_3$ are principal stretches, and I_1, I_2, I_3 are the invariants of left Cauchy-Green strain tensor, **B**, respectively, obtained as:

$$I_1 = trace\,(\boldsymbol{B}) \quad (3)$$

$$I_2 = \frac{1}{2}\,(I_1^2 - \boldsymbol{B}\cdot\boldsymbol{B}) \quad (4)$$

$$I_3 = det\,(\boldsymbol{B}) \quad (5)$$

In hyperelastic models the Cauchy stresses are derived by differentiating the strain energy density function as follows:

$$\sigma = \frac{2}{J}\cdot\boldsymbol{B}\cdot\frac{\partial W}{\partial \boldsymbol{B}} = \frac{1}{J}\cdot\frac{\partial W}{\partial \boldsymbol{F}}\cdot\boldsymbol{F}^T \quad (6)$$

where **F** is the strain gradient tensor and J=det (**F**).

In this paper, five different constitutive models have been used:

- Linear elastic model
- Hyperelastic Neo Hookean model
- Hyperelastic Mooney-Rivlin model
- Hyperelastic Ogden model
- Hyperelastic Marlow model

4.1. Linear elastic model

In this model the material returns to its original shape when the loads are removed, and the unloading path is the same as the loading path. This model is known as Hooke's Law. The stress is proportional to the strain and the constant of proportionality is the Young's modulus (E).

$$\sigma = E\cdot\varepsilon \quad (7)$$

The strain energy density functions is defined as:

$$W = \frac{1}{2}\cdot\sigma_{ij}\cdot\varepsilon_{ij} \quad (8)$$

4.2. Hyperelastic Neo Hookean model

This model was proposed by Treloar in 1943 (Treloar, L R.G., 1943). In this model, the strain energy density function is based only on the first strain invariant:

$$W = C_1(I_1 - 3) + \frac{1}{D}(J-1)^2 \quad (9)$$

where C_1 is a material constant, J is the determinant of the strain gradient tensor **F** and D is a material constant related to the bulk modulus.

4.3. Hyperelastic Mooney-Rivlin model

The Mooney-Rivlin model (Mooney, 1940) (Rivlin, R. S. and Saunders, D. W., 1951), proposed in 1951, is one of the most used hyperelastic models in the literature. Although there are various versions of this model, the most general is based on the first and second strain invariants. The strain energy density function is defined as follows:

$$\mathrm{W} = \mathrm{C}_{10}(\mathrm{I}_1 - 3) + \mathrm{C}_{01}(\mathrm{I}_2 - 3) + \frac{1}{\mathrm{D}}(\mathrm{J}-1)^2 \quad (10)$$

where C_{ij} are material constants, J is the determinant of the strain gradient tensor **F** and D is a material constant related to the bulk modulus. Neo Hookean is a particular case of the two parameters Mooney-Rivlin model.

4.4. Hyperelastic Ogden model

The Ogden hyperelastic model (1972) (Ogden, R. W., 1972) is possibly the most extended model after Mooney-Rivlin model. This model is based on the three principal stretches (λ_1, λ_2, λ_3) and 2N material constants, where N is the number of polynomials that constitute the strain energy density function, defined as:

$$W = \sum_{i=1}^{N}\frac{\mu_i}{\alpha_i}\left(\lambda_1^{\alpha_i} + \lambda_2^{\alpha_i} + \lambda_3^{\alpha_i} - 3\right) + \sum_{k=1}^{N}\frac{1}{D}(J-1)^{2k} \quad (11)$$

where μ_i y α_i are material constants, J is the determinant of the strain gradient tensor **F** and D is a material constant related to the bulk modulus.

4.5. Hyperelastic Marlow model

The Marlow hyperelastic model (2003) (Marlow, R. S. , 2003) means the strain energy density is independent of the second invariant, and a single test such as a uniaxial

tension test is necessary to determine the material response. The strain energy density function is defined as:

$$W = \int_0^{\lambda_T - 1} T(\varepsilon) d\varepsilon \tag{12}$$

where T(ε) is the nominal uniaxial stress and λ_T is the uniaxial stretch.

4.6. Fitting parameters of material models

For all the previously presented models, the optimal constant values were obtained by means of an optimization algorithm to try to faithfully reproduce the material behaviour provided by the manufacturer. A least squares algorithm was used to minimize this variable. The error function is defined as:

$$\text{Error} = \sum_{i=1}^{m} (\text{Data}_{\text{real}} - \text{Data}_{\text{model}})^2 \tag{13}$$

where m is the number of points on the chart provided by the manufacturer.

Since the minimum principal strain provided on the component is about -14% and the maximum principal strain is 20%, the models have been adjusted to this range of strain.

Once the optimal constant values were obtained, for each model, the strain energy density and the strain-stress curves were obtained and they were compared with the actual material curves. To determine the quality of each of the models, the R^2 correlation coefficient was calculated for the strain-stress plot (Figure 7).

The values of material parameters and R^2 values for the models are shown in Table 4.

Table 4: Parameters and R^2 values of models

Model	Parameter	Optimal Value	R^2
Linear elastic	E	14.602	0.978
Hyperelastic Neo Hookean	C_1	2.416	0.977
Hyperelastic Mooney Rivlin	C_{10}	3.190	0.975
	C_{01}	-0.818	
Hyperelastic Ogden N=2	μ_1	25.560	0.977
	α_1	0.065	
	μ_2	76.579	
	α_2	0.108	

In view of the obtained results, all presented models fit well with actual values of the material datasheet because the R^2 correlation coefficient is always higher than 0.960. Therefore any of the studied models should provide good results in the simulation of the component.

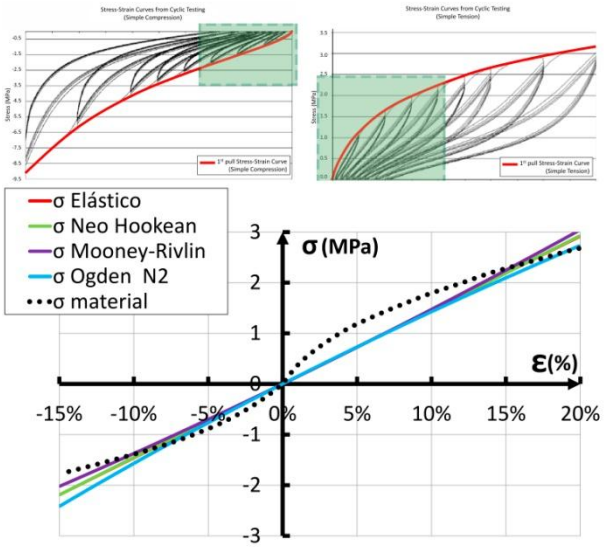

Figure 7: Strain-stress plot for different models between -14% and 20% strain

5. SIMULATIONS AND RESULTS

In order to check the mechanical behavior of the component depending on the constitutive model used, five finite element simulations of the duct compression were performed. Each of them uses one of the different material constitutive models introduced in Section 3.

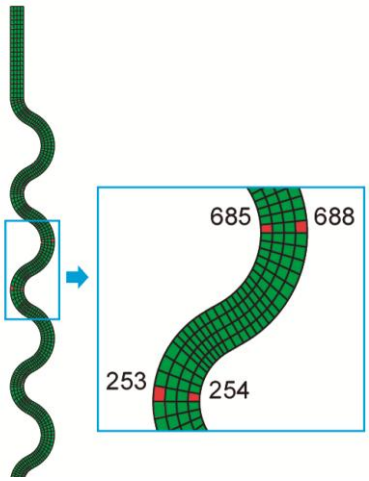

Figure 8: Four characteristic elements of the model

The values of the variables most commonly used in the engineering field, like stresses, strains and energy, have been obtained from integration points of four characteristic elements of the model (Figure 8).

In several studies maximum principal strain and the strain energy density were used to evaluate the life of component when a cyclic load was applied to it. (Mars, W. V., & Fatemi, A., 2002). Other investigations about fatigue use maximum principal stresses to calculate the life of component. (André, N., Cailletaud, G., & Piques, R., 1999). Finally, the Von Mises comparison stress is commonly used to know if the material is able to resist a static load or displacement.

So, concerning the strain field, the maximum and the minimum principal strains, respectively, were studied (Figures 9 and 10). On the other hand, for the stress field, the maximum and minimum principal stresses, respectively, (Figures 11 and 12) and the von Mises stress were analyzed (Figure 13) at each of the integration points and these values were referred at centroid of elements. And finally, the strain energy density was also studied (Figure 14).

6. DISCUSSION

The obtained results show that the mechanical behavior of Santoprene 101-73 can be accurately adjusted by using the different models of hyperelastic behavior considered with the appropriate material constants, with a good agreement with the data supplied by the manufacturer for the uniaxial stress-strain curve. A least squares algorithm allows obtaining the material constant reaching values of R^2 over 0.975 in all studied models when applied for stress-strain uniaxial curve.

However, important differences were found in stresses (up to 40%) and the strain energy density (up to 90%) when the models were applied to a real component in a wide range of strain as occurs in the normal operation of that kind of pieces.

To this respect, the pure elastic, the NeoHookean, the Mooney-Rivlin and the Ogden models provide similar results as much in principal strains as in principal stresses. A similar trend is observed for von Mises stress and strain energy density.

A more realistic behavior is obtained by using Marlow model and important divergences were found respect the other models. The divergence is more pronounced for stresses and strain energy density, whereas it is considerably lesser for strains.

So, a careful election of the appropriate constitutive model must be done in order to obtain realistic simulations of real components, in such a way that the results corresponding to strains and stresses would be reliable enough, allowing the strength and functionality verifications, considering that those magnitudes are used to predict mechanical performance, fatigue life, etc., and then can determine important features of the component design.

7. CONCLUSIONS

The aim of this paper was to determine the best constitutive model for reproducing the mechanical behavior of Santoprene 101-73, material used in automotive industry. To reach it, four different hyperelastic models and the commonly used linear elastic model have been studied in order to obtain the material constants of each of them. An optimization least squares algorithm were used to fit the best values of material constants to each of them. In order to conclude which of them best represents the actual behavior of the material, the R^2 correlation coefficient for stress-strain relationship has been used.

In view of the obtained results, it can be concluded that all the considered models fit the actual material behavior with enough accuracy, being the Marlow model the most accurate model to reproduce the mechanical behavior of Santoprene 101-73, considering the stress-strain uniaxial curve.

However, the study has demonstrated that despite using constitutive models that fit correctly to the actual behavior of the material in standardized uniaxial tests, the different models show large differences concerning the realistic behavior when they are applied to real components, in which complex stress/strain fields can arise. So, more information from biaxial and planar tests is needed in order to perform accurate simulations for real components.

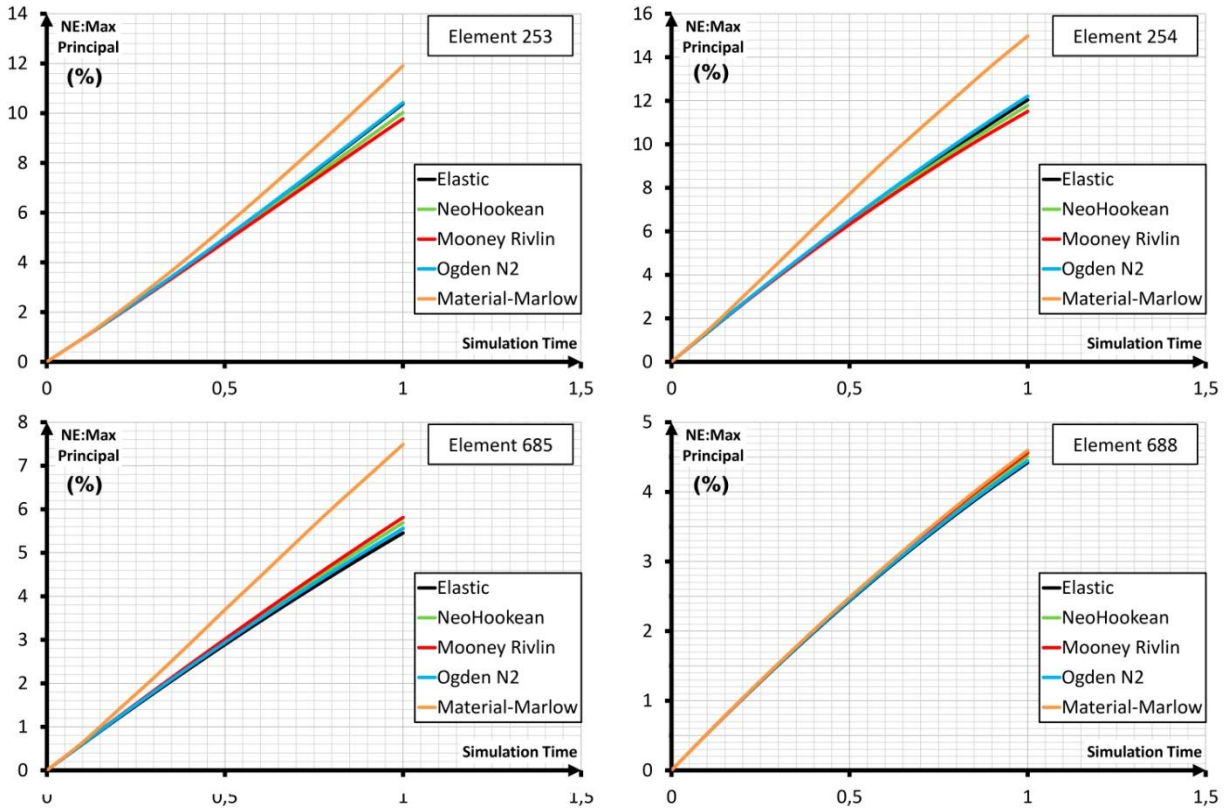

Figure 9: Maximum principal strain for different models calculated at each of the integration points and referred at centroid of four characteristic elements.

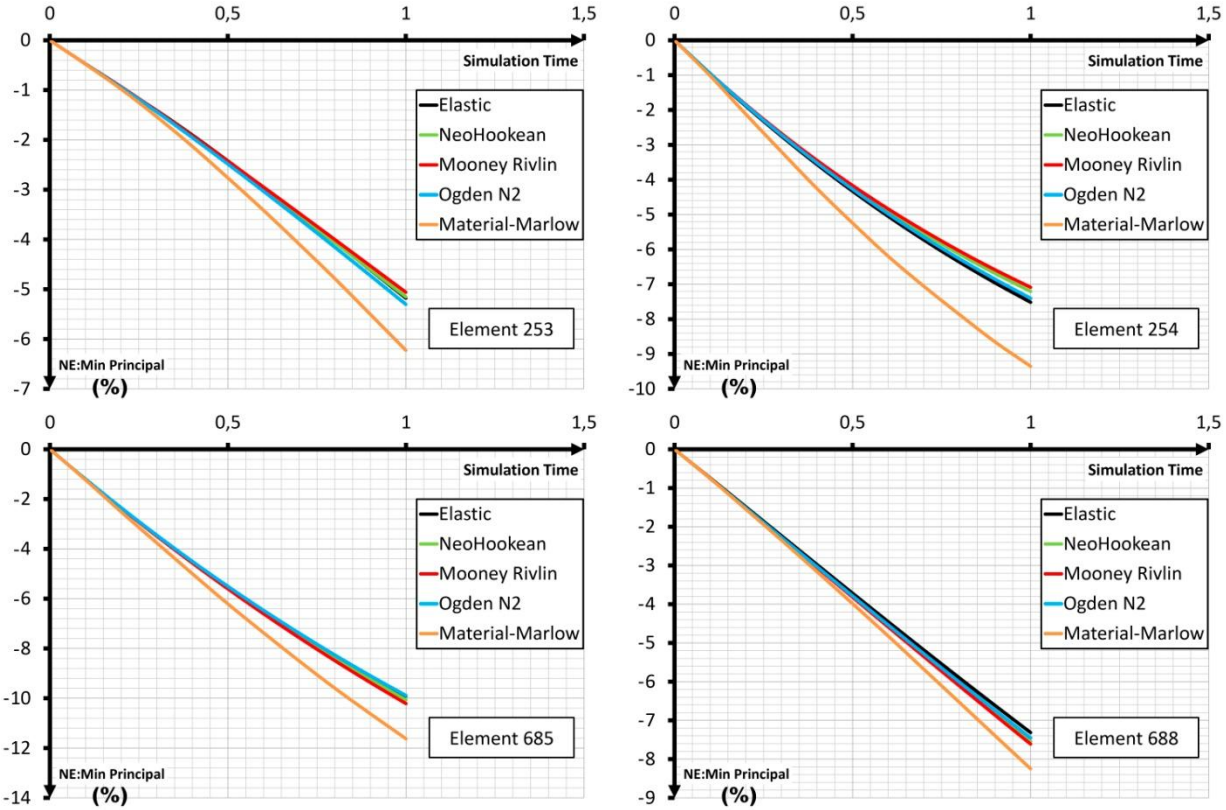

Figure 10: Minimum principal strain for different models calculated at each of the integration points and referred at centroid of four characteristic elements.

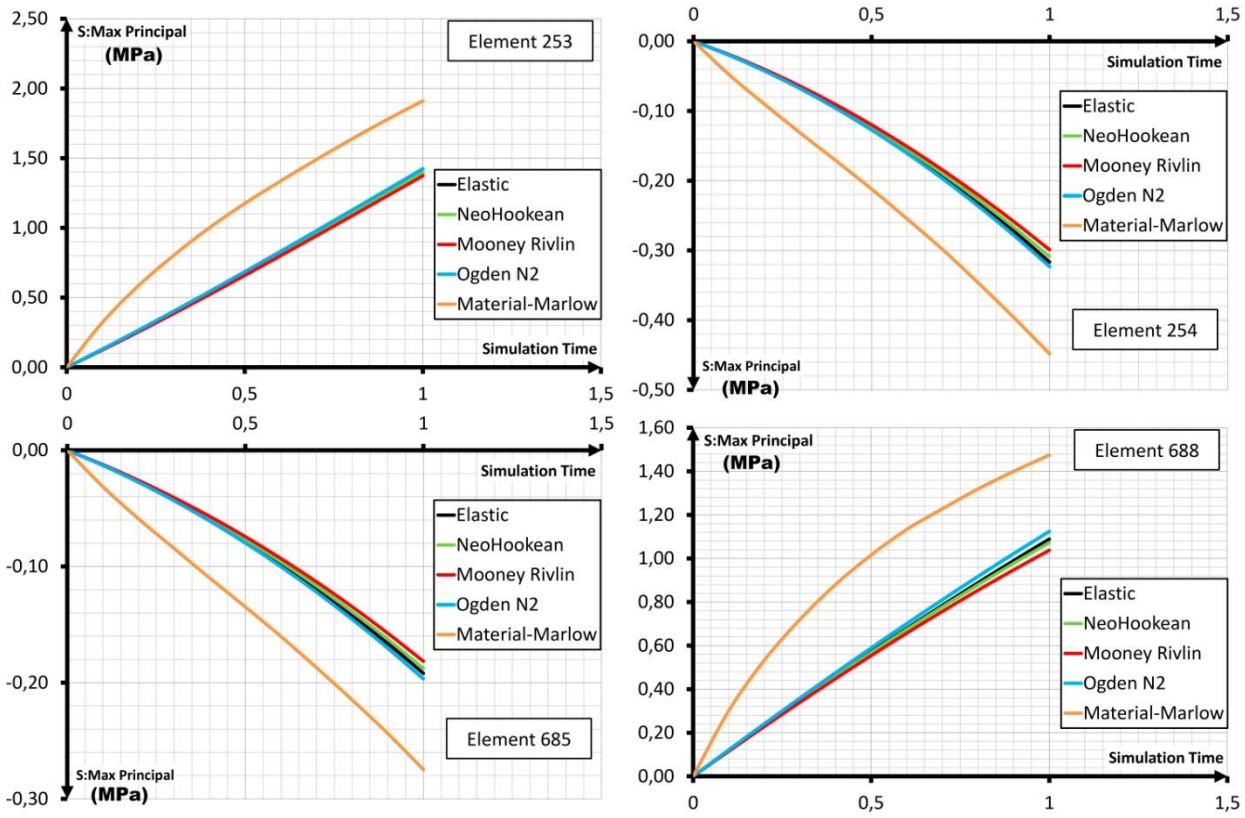

Figure 11: Maximum principal stress for different models calculated at each of the integration points and referred at centroid of four characteristic elements.

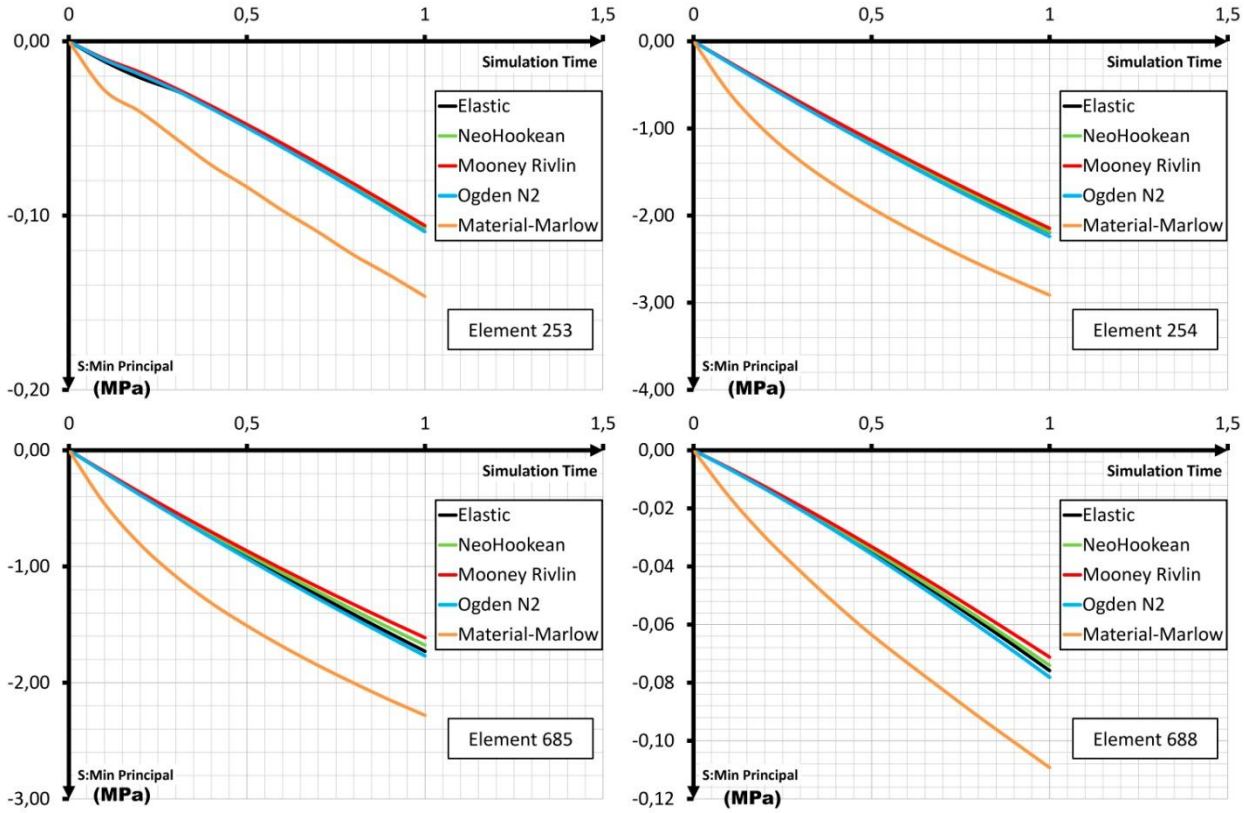

Figure 12: Minimum principal stress for different models calculated at each of the integration points and referred at centroid of four characteristic elements.

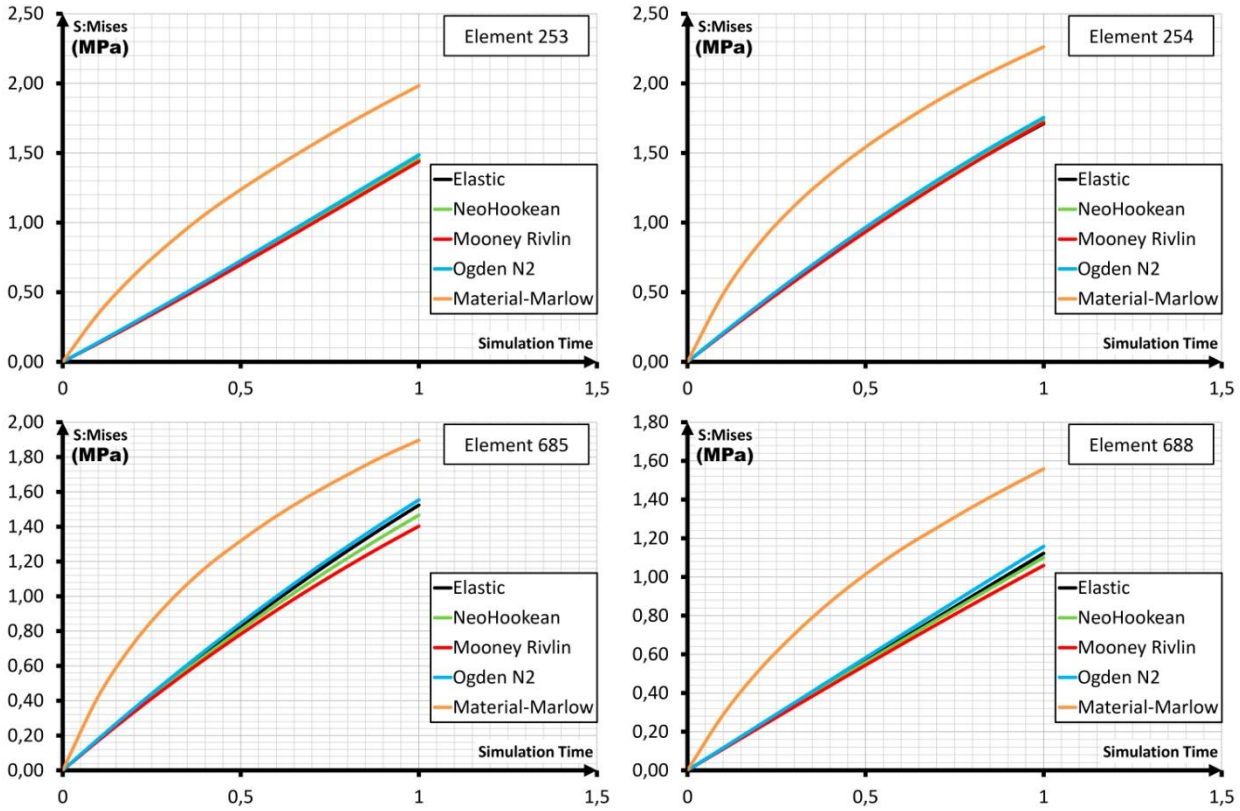

Figure 13: Von Mises comparison stress for different models calculated at each of the integration points and referred at centroid of four characteristic elements.

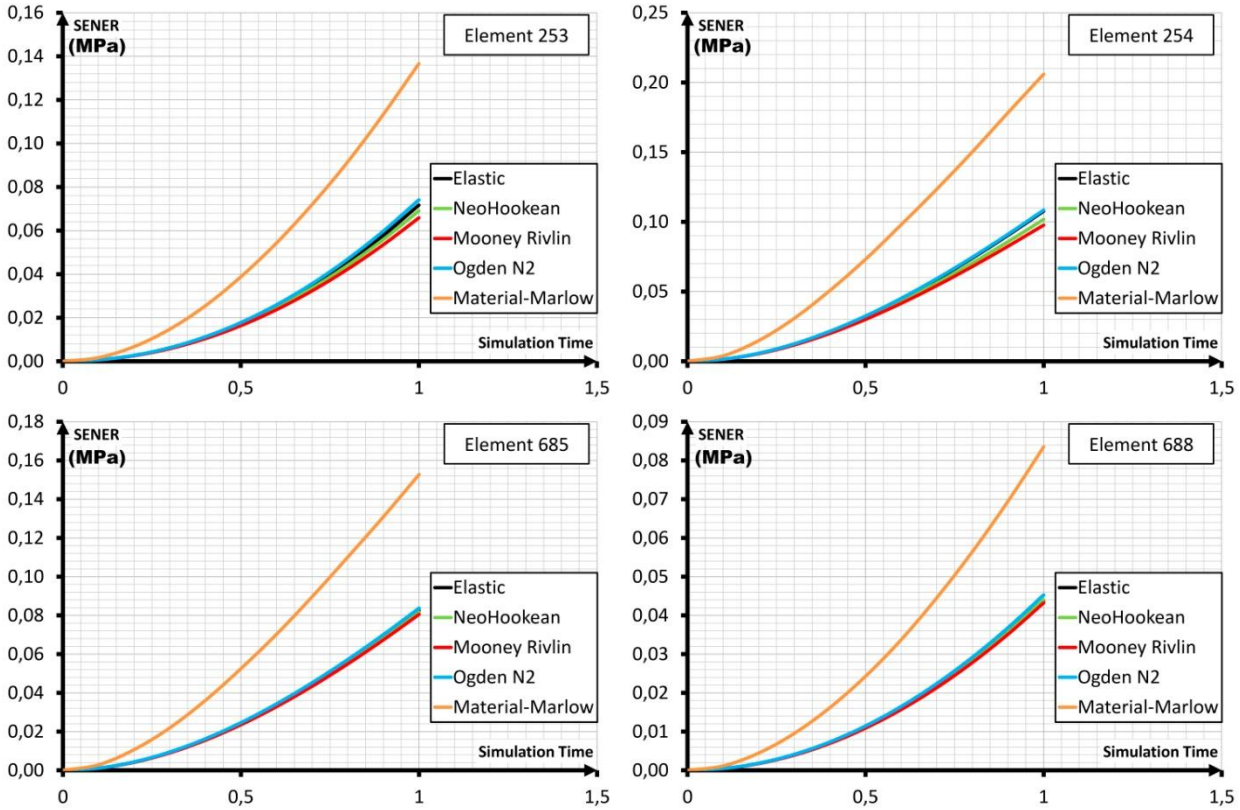

Figure 14: Strain energy density (SED) for different models calculated at each of the integration points and referred at centroid of four characteristic elements.

REFERENCES

Abaqus Analysis User's Manual, Abaqus 6.11 Online Documentation, Dassault Systèmes, 2011.

André, N., Cailletaud, G., & Piques, R. (1999). Haigh diagram for fatigue crack initiation prediction of natural rubber components. Kautschuk Gummi Kunststoffe, 52(2), 120-123.

ASTM D412-15a, Standard Test Methods for Vulcanized Rubber and Thermoplastic Elastomers—Tension, ASTM International, West Conshohocken, PA, 2015, www.astm.org

Charlton, D. J., Yang, J., The, K K., A Review of Methods to Characterize Rubber Elastic Behavior for Use in Finite Element Analysis, Rubber Chemistry and Technology (3) 481–503.1994

Drobny, J. G. (2014). Handbook of thermoplastic elastomers. Elsevier.

Dufton, P. W. (2001). Thermoplastic Elastomers Market. iSmithers Rapra Publishing.

ExxonMobil, Santoprene 101-73 Thermoplastic Vulcanizate.

Fernández, A., Javierre, C., González, J. & Elduque, D., 2013. Development of thermoplastic material food packaging considering technical, economic and environmental criteria. *Journal of Biobased Materials and Bioenergy*, 7(2), 176-183.

ISO 37:2011. Rubber, vulcanized or thermoplastic – determination of tensile stress–strain properties. ISO Standard; 2011.

Javierre, C., Abad-Blasco, J., Camañes & V., F. D., 2013. Redesign of metalic parts with thermoplastic materials: Application example | Rediseño de componentes metálicos En materiales termoplásticos: Ejemplo de aplicación. *DYNA*, 88(2), 197-205.

Javierre, C., Elduque, D., Camañes, V. & Franch, D. (2014). Simulation and experimental analysis of led weather proof luminaire thermal performance. *Paper presented at the 26th European Modeling and Simulation Symposium, EMSS 2014.*

Javierre, C., Fernández, A., Aísa, J. & Clavería, I., 2006. Criteria on feeding system design: Conventional and sequential injection moulding. *Journal of Materials Processing Technology*, 171(3), 373-384.

Jiménez, E. et al. 2014. Methodological approach towards sustainability by integration of environmental impact in production system models through life cycle analysis: Application to the Rioja wine sector. *SIMULATION*, 90(2), pp.143-161.

Jiménez, E., Ruiz, I., Blanco, J., & Pérez, M. (2009). Design and simulation of production of injection pieces in automobile industry. International *Journal of Simulation: Systems, Science and Technology*, 10(3), 23-30.

Kutz, M. (Ed.). (2011). Applied plastics engineering handbook: processing and materials. William Andrew.

Latorre-Biel, J. I., Jiménez-Macías, E., Blanco-Fernández, J., & Sáenz-Díez, J. C. (2013b). Optimal design, based on simulation, of an olive oil mill. *Paper presented at the 25th European Modeling and Simulation Symposium, EMSS 2013.*

Mars, W. V., & Fatemi, A. (2002). A literature survey on fatigue analysis approaches for rubber. International Journal of Fatigue, 24(9), 949-961.

Marlow, R. S. (2003). A general first-invariant hyperelastic constitutive model. *Constitutive Models for Rubber*, 157-160.

Mooney, M. (1940). A theory of large elastic deformation. *Journal of applied physics*, *11*(9), 582-592.

Ogden, R. W. (1972, February). Large deformation isotropic elasticity-on the correlation of theory and experiment for incompressible rubberlike solids. In Proceedings of the Royal Society of London A: Mathematical, Physical and Engineering Sciences (Vol. 326, No. 1567, pp. 565-584). The Royal Society.

P. Consulting, Global elastomeric polyolefins markets, technologies trends (2014) 2014–2020.

Rivlin, R. S., & Saunders, D. W. (1951). Large elastic deformations of isotropic materials. VII. Experiments on the deformation of rubber. Philosophical Transactions of the Royal Society of London A: Mathematical, Physical and Engineering Sciences, 243(865), 251-288.

Robert A.. Malloy. (1994). Plastic part design for injection molding: an introduction. Hanser Publishers.

Ruiz Argáiz, I., Jiménez Macías, E., Blanco Fernández, J., & Pérez de la Parte, M. (2008). Design and simulation of production of injection pieces in automobile industry. Paper presented at the *Proceedings -EMS 2008, European Modelling Symposium, 2nd UKSim European Symposium on Computer Modelling and Simulation.*

Štrumberger, N., Gospočić, A., & Bartulić, Č. (2012). Polymeric Materials in Automobiles. PROMET-Traffic&Transportation, 17(3), 149-160.

Treloar, L. R. G. (1943). The elasticity of a network of long-chain molecules—II. *Transactions of the Faraday Society*, *39*, 241-246.